Cell Stem Cell
Short Article

Acute Myelogenous Leukemia-Induced Sympathetic Neuropathy Promotes Malignancy in an Altered Hematopoietic Stem Cell Niche

Maher Hanoun,[1,2] Dachuan Zhang,[1,2] Toshihide Mizoguchi,[1,2] Sandra Pinho,[1,2] Halley Pierce,[1,2] Yuya Kunisaki,[1,2] Julie Lacombe,[1,2] Scott A. Armstrong,[4] Ulrich Dührsen,[5] and Paul S. Frenette[1,2,3,*]
[1]Ruth L. and David S. Gottesman Institute for Stem Cell and Regenerative Medicine Research, Albert Einstein College of Medicine, Bronx, NY 10461, USA
[2]Department of Cell Biology, Albert Einstein College of Medicine, Bronx, NY 10461, USA
[3]Department of Medicine, Albert Einstein College of Medicine, Bronx, NY 10461, USA
[4]Human Oncology and Pathogenesis Program, Memorial Hospital Research Laboratories, Memorial Sloan Kettering Institute, New York, NY 10065, USA
[5]Department of Hematology, University Hospital, University Duisburg-Essen, Hufelandstrasse 55, 45122 Essen, Germany
*Correspondence: paul.frenette@einstein.yu.edu
http://dx.doi.org/10.1016/j.stem.2014.06.020

SUMMARY

Perivascular mesenchymal stem and progenitor cells (MSPCs) are critical for forming a healthy hematopoietic stem cell (HSC) niche. However, the interactions and influence of acute myelogenous leukemia (AML) stem cells with the microenvironment remain largely unexplored. We have unexpectedly found that neuropathy of the sympathetic nervous system (SNS) promotes leukemic bone marrow infiltration in an *MLL-AF9* AML model. Development of AML disrupts SNS nerves and the quiescence of Nestin$^+$ niche cells, leading to an expansion of phenotypic MSPCs primed for osteoblastic differentiation at the expense of HSC-maintaining NG2$^+$ periarteriolar niche cells. Adrenergic signaling promoting leukemogenesis is transduced by the β2, but not β3, adrenergic receptor expressed on stromal cells of leukemic bone marrow. These results indicate that sympathetic neuropathy may represent a mechanism for the malignancy in order to co-opt the microenvironment and suggest separate mesenchymal niche activities for malignant and healthy hematopoietic stem cells in the bone marrow.

INTRODUCTION

Understanding the mechanisms by which the hematopoietic stem cell (HSC) niche regulates leukemia-initiating cells, also referred to as leukemia stem cells (LSCs), in acute myelogenous leukemia (AML) is crucial to improving treatment outcome and eradicating the disease. Expansion of the leukemic clone is associated with the impairment of normal hematopoiesis, resulting in severe anemia, thrombocytopenia, and immunodeficiency, which can lead to severe morbidity in affected individuals (reviewed in Ferrara and Schiffer, 2013). Additionally, a high relapse rate in AML suggests that quiescent LSCs are not targeted by currently used treatment protocols (Byrd et al., 2002; Ishikawa et al., 2007). However, little is known about the underlying mechanisms that cause the severe hematopoietic failure in AML and how LSCs alter the bone marrow microenvironment.

Recent studies have demonstrated that healthy HSCs reside in specific perivascular bone marrow niches, which tightly regulate their function (reviewed in Frenette et al., 2013). Several candidate niche cells have been suggested, including CXCL12-abundant reticular cells (Sugiyama et al., 2006), Nestin$^+$ (Nes$^+$) cells (Méndez-Ferrer et al., 2010), and Leptin receptor (LepR)$^+$ cells (Ding et al., 2012), that exhibit significant overlap among each other (Pinho et al., 2013). Vascular structures were recently found to form distinct niches where arterioles marked by *Nes*-GFP^{bright} NG2$^+$ pericytes were associated with dormant HSCs, whereas reticular-shaped sinusoidal *Nes*-GFP^{dim} cells were associated with less-quiescent HSCs (Kunisaki et al., 2013). Arterioles of the bone marrow are highly innervated by neural fibers of the sympathetic nervous system (SNS) that regulate HSC migration (Katayama et al., 2006; Méndez-Ferrer et al., 2008). Input from SNS nerves is also critical for bone marrow regeneration after genotoxic insults where SNS neuropathy can impair HSC recovery after irradiation or 5-fluorouracil-induced damage (Lucas et al., 2013).

To what extent LSCs share properties with healthy HSCs remains unclear. Furthermore, the heterogeneity among acute leukemias suggests the potential for differential requirements by the bone marrow microenvironment. In keeping with this idea, expression of different cytokines in the bone marrow can direct human MLL-AF9 leukemia into either AML or B cell acute lymphogenous leukemia (ALL) fate (Wei et al., 2008). MLL-AF9 AML cells have been suggested to home further away from the bone in comparison to healthy HSCs and do not rely on niche-derived Wnt signals (Lane et al., 2011). In a xenograft model of ALL, infiltration of leukemic cells altered the homing sites of healthy CD34$^+$ progenitors (Colmone et al., 2008). *BCR-ABL*-driven chronic myelogenous leukemia (CML) was reported to alter the microenvironment and reduce the capacity to support normal hematopoiesis (Schepers et al., 2013; Zhang et al., 2012). Conversely, patient-derived mesenchymal stem and progenitor cells (MSPCs) were shown in order to propagate the

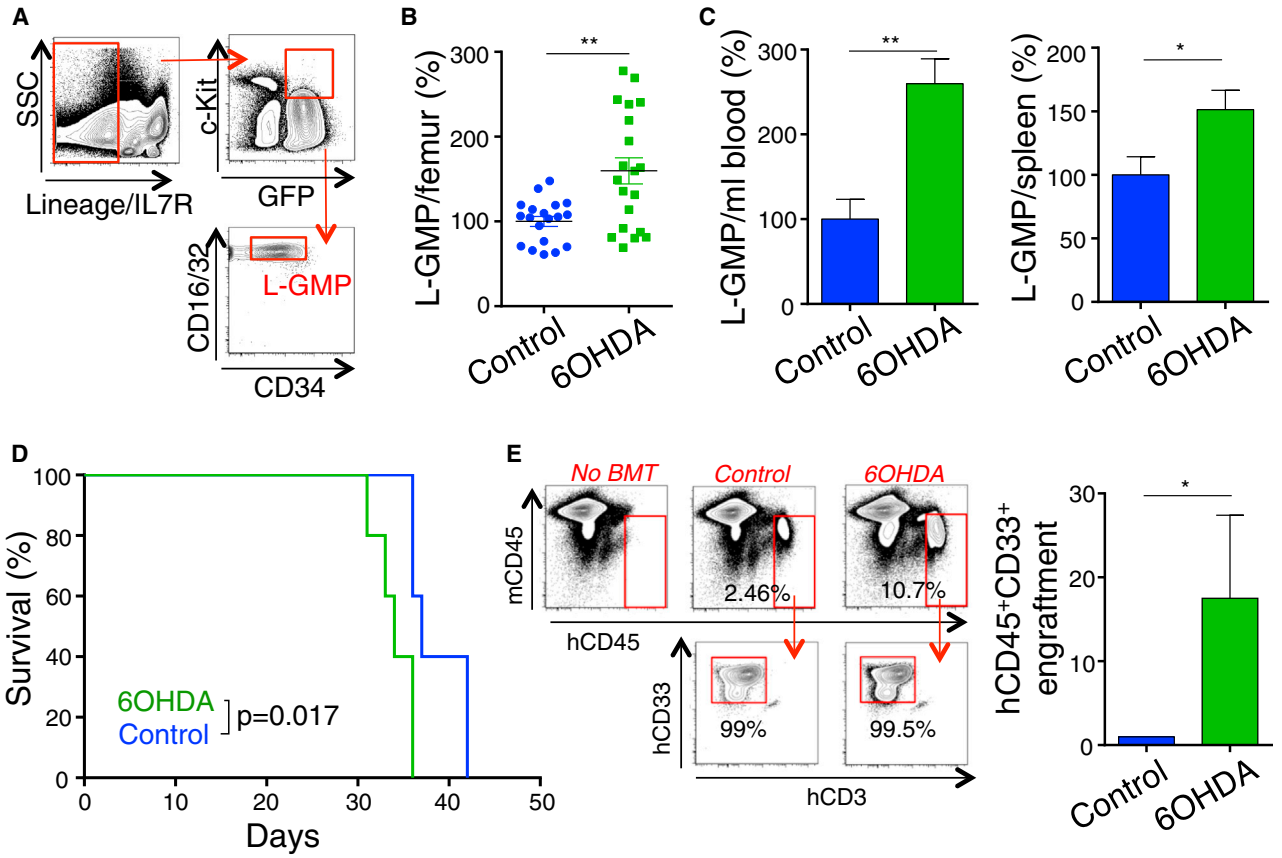

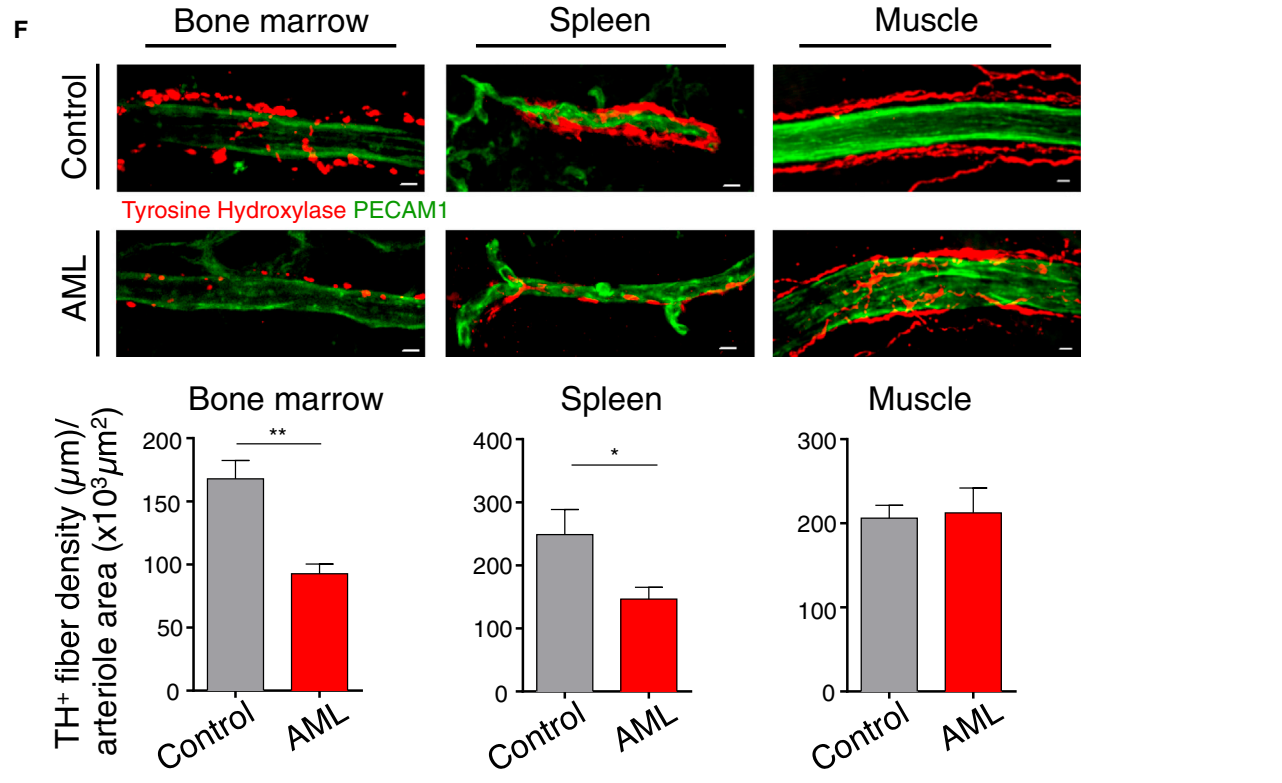

(legend on next page)

expansion of human myelodysplastic cells in xenografts (Medyouf et al., 2014). However, the nature of the LSC niche remains unclear.

Given the rapid and extensive remodeling imposed by AML infiltration of the bone marrow, we anticipated that the mechanisms of bone marrow regeneration might overlap with the requirements of AML development. The importance of SNS nerve function in hematopoietic regeneration (Lucas et al., 2013) combined with the requirement of SNS nerves for the development of xenografted prostate cancer (Magnon et al., 2013), suggested that the inhibition of adrenergic signals might curb AML development. Unexpectedly, we report herein that MLL-AF9 AML co-opts SNS fibers in the bone marrow and spleen and that sympathetic neuropathy or adrenergic blockade promotes AML through an expanded, but severely altered, stem cell niche.

RESULTS

Adrenergic Signals Regulate AML

We transduced Lin$^-$c-Kit$^+$Sca-1$^+$ (LSK) cells with the *MLL-AF9* oncogene and clonally propagated transduced LSK cells in methylcellulose as preleukemic cells (Krivtsov et al., 2006). Transplantation of transduced cells rapidly induced the disease with massive bone marrow and spleen infiltration of monomorphic undifferentiated cells uniformly expressing myeloid cell markers, without myelofibrosis (data not shown). Serial transplantations enriched for stem cell activity and robust engraftment could be reproducibly achieved with leukemic bone marrow cells from tertiary recipients without the need for preconditioning and avoiding the potential of irradiation-induced changes in the microenvironment.

To assess the functional role of the SNS in AML, we ablated adrenergic nerves of recipient mice with 6-hydroxydopamine (6OHDA), which specifically disrupts catecholaminergic neurons without directly affecting hematopoietic cells (Katayama et al., 2006; Méndez-Ferrer et al., 2008). Surprisingly, we found that mice with denervated bone marrow exhibited greater infiltration by phenotypic LSCs, defined as IL-7R$^-$Lin$^-$GFP$^+$c-Kit^{hi}CD34^{lo} FcγRII/III^{hi} granulocyte-macrophage progenitors (L-GMPs) (Figures 1A and 1B), and significantly higher egress of L-GMPs to peripheral blood and spleen than control animals (Figure 1C). This was associated with a significant reduction in the survival of denervated leukemic mice after transplantation of either preleukemic or leukemic MLL-AF9 cells (Figures 1D; Figure S1A available online). These significant differences in leukemia development were due to neither a potential effect of denervation on the homing of leukemic cells to bone marrow and spleen (Figure S1B) nor a direct effect on MLL-AF9 leukemia cells (Figure S1C). Furthermore, sympathetic denervation performed after the leukemic cell injection significantly accelerated the course of disease, indicating that adrenergic regulation of AML acted beyond the engraftment period (Figure S1D). We did not observe any difference between the two groups in cell cycle or apoptosis of LSCs after transplantation (Figures S1E and S1F). Thus, bone marrow infiltration by AML is increased when sympathetic innervation is compromised.

To assess the relevance of adrenergic signals in human AML, we transplanted primary human AML cells into denervated and control NOD-*scid* IL2R$\gamma^{-/-}$ mice. We observed a significantly higher bone marrow infiltration with human myeloid cells in denervated mice (Figure 1E), even when samples were derived from myeloblastic or myelomonocytic leukemia (French-American-British classification AML M1 or M4), suggesting that the SNS may affect AML outside the MLL-AF9$^+$ monocytic subtype.

To get more insight into the effect of AML infiltration on the HSC niche, we injected MLL-AF9 leukemic cells into *Nes*-Gfp$^+$ mice in which GFP expression by perivascular cells marks HSC niches (Méndez-Ferrer et al., 2010). After 3 weeks, we evaluated the bone marrow by immunofluorescence imaging of thick sections in order to assess the vascular structures (Kunisaki et al., 2013). Leukemic bone marrow exhibited marked increases in sinusoidal densities with a disorganized appearance (Figure 2F). Additionally, tyrosine hydroxylase (TH) staining, which specifically labels catecholaminergic fibers, revealed a significant reduction of arterioles covered by TH$^+$ fibers in AML bone marrow in comparison to healthy controls (data not shown). Strikingly, the arterioles that remained innervated exhibited significant reductions in the density of ensheathing TH$^+$ fibers (Figure 1F, left). Sympathetic neuropathy was not confined to the bone marrow but also occurred in the spleen, and this correlated with reduced noradrenaline levels in these tissues (Figures 1F, middle, and S1G). In contrast, adrenergic innervation of the skeletal muscle, a site which is not primarily infiltrated by leukemic cells, did not exhibit any significant change (Figure 1F, right). These results indicate that leukemia development induces sympathetic neuropathy at infiltrated sites, resulting in a locally reduced sympathetic tone which in turn may reinforce the leukemic disease.

Figure 1. Sympathetic Neuropathy Promotes Leukemogenesis

(A) Gating strategy for flow cytometry analysis of LSC/L-GMPs.

(B) Absolute number of L-GMPs per femur in control and denervated leukemic mice 20 days after transplantation (normalized to control, n = 19–20).

(C) Absolute number of L-GMPs per ml blood (left) and spleen (right) in control and denervated leukemic mice 23 days after transplantation (normalized to control, n = 4–5).

(D) Survival curve of control and denervated leukemic mice (n = 5).

(E) Left, flow cytometry gating strategy for bone marrow analysis of human hematopoietic engraftment by gating on human (h) CD45$^+$ cells detecting exclusively myeloid hCD33$^+$ cells and excluding hCD3$^+$ and hCD19$^+$ expression (data not shown). Representative flow cytometry plots from each experimental condition (BMT = bone marrow transplantation). Right, human myeloid bone marrow engraftment 4 weeks after transplantation of primary human AML cells in control or denervated NSG mice (data are normalized to paired controls, n = 4 human AML samples).

(F) Top, z stack confocal images from bone marrow, spleen, and cremaster muscle stained for PECAM1$^+$ endothelial cells and TH$^+$ nerve fibers. The scale bar represents 10 μm. Bottom, assessment of the TH$^+$ fiber density per arteriole by quantifying the total length of all TH$^+$ branches divided by the area of the corresponding arteriole (bone marrow: n = 33–49 arterioles from six to eight mice per group; spleen n = 21–29 arterioles from five mice per group; cremaster muscle: n = 16–17 arterioles from six mice per group). *p < 0.05, **p < 0.01 determined by Student's t test. Data are shown as mean ± SEM.

See also Figure S1.

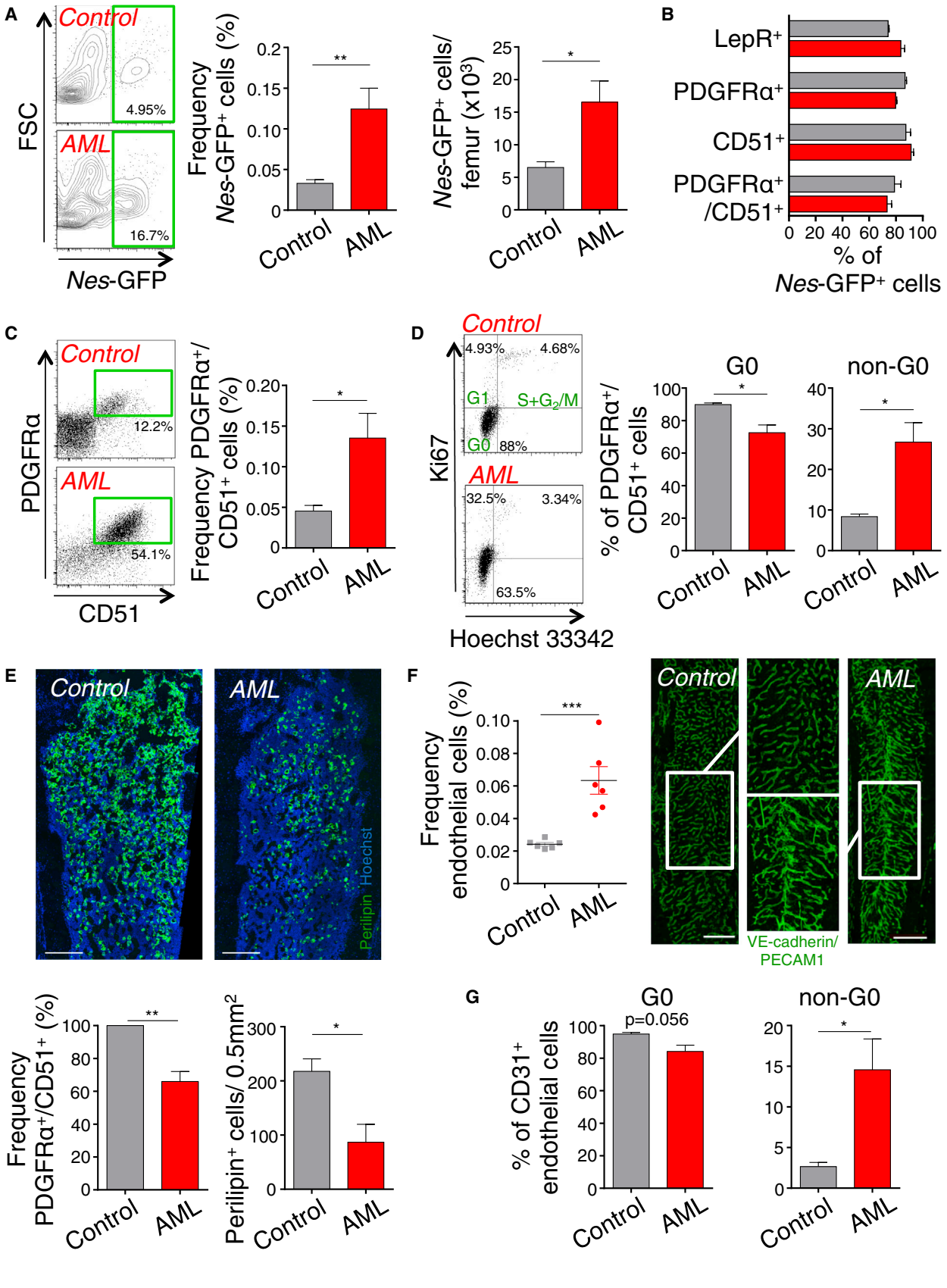

(legend on next page)

Because our recent studies have revealed that the denervation of healthy bone marrow can lead to increased numbers of *Nes*-GFP$^+$ cells (Lucas et al., 2013), we determined the content of stromal and endothelial cells with fluorescence-activated cell sorting (FACS). We found a ~3.8-fold expansion of *Nes*-GFP$^+$ bone marrow stromal (CD45$^-$CD11b$^-$Ter119$^-$CD31$^-$) MSPCs in leukemic mice (Figures 2A). Leukemic bone marrow *Nes*-GFP$^+$ cells retained their phenotypic characteristics with similar proportion of LepR$^+$, PDGFRα^+, and CD51$^+$ cells than healthy control mice (Figures 2B). The increased numbers of PDGFRα^+CD51$^+$ MSPCs (Pinho et al., 2013) confirmed that the higher proportion of *Nes*-GFP$^+$ cells was not due to an effect of the leukemia on the *Nes* promoter activity (Figure 2C). MSPCs exhibited a significant loss of quiescence, suggesting that their increased numbers were most likely due to proliferation (Gronthos et al., 2003; Kunisaki et al., 2013) (Figure 2D).

The loss of quiescence resulted in a higher vulnerability to genotoxic insult. In control mice, sublethal irradiation can induce adipogenesis in the bone marrow (Bryon et al., 1979), through differentiation from MSPCs (Mizoguchi et al., 2014). However, in leukemic mice, the number of MSPCs was significantly reduced after irradiation, resulting in reduced numbers of Perilipin$^+$ adipocytes (Figure 2E). In line with increased vascular densities (Figure 2F) (see also Aguayo et al., 2000; Hussong et al., 2000; Padró et al., 2000), leukemic bone marrow contained increased numbers of endothelial cells as determined by flow cytometry (Figure 2F) and cell-cycle analyses also revealed a reduction of the quiescent fraction (Figures 2G). These results indicate that leukemic bone marrow infiltration leads to MSPC and endothelial cell expansion associated with SNS denervation.

Expanded *Nes*-GFP$^+$ Cells Are Directed Toward the Osteoblastic Lineage

We assessed the function of mesenchymal lineages in leukemic bone marrow. Purified *Nes*-GFP$^+$ cells from leukemic marrow contained a 1.7-fold greater fibroblastic colony-forming unit (CFU-F) capacity in comparison to healthy controls (Figure 3A) but remained confined within the *Nes*-GFP$^+$ stromal population (data not shown). To assess the commitment of *Nes*-GFP$^+$ cells to differentiate to the osteoblastic lineage, we stimulated osteoblast differentiation and mineralization in isolated *Nes*-GFP$^+$ bone marrow cells. We found a significant increase in the number of osteoblastic colony-forming units (CFU-OB) with larger mineralizing colonies, indicating that *Nes*-GFP$^+$ cells in leukemic bone marrow have an enhanced commitment toward osteoblastic differentiation (Figures 3B and 3C). A subset of leukemic bone-marrow-derived *Nes*-GFP$^+$ cells showed multilineage differentiation capacity after >30 days in culture (Figure S2A). In line with these data, the number of immature and mature osteolineage cells from the compact bone, measured as CD51$^+$/Sca-1$^-$ stromal cells (Winkler et al., 2010), were significantly increased in AML (Figure 3D). However, we found that tartrate-resistant acid phosphatase (TRAP)$^+$ osteoclast numbers in the metaphysis of the tibiae of diseased leukemic mice were reduced (Figure 3E). To morphologically characterize these osteolineage cells, we transplanted *Osterix (Osx)-cre^{ERT2}/loxp-tdTomato* mice with MLL-AF9 leukemic cells. Consistent with prior analyses, Cre-mediated recombination in 8-week-old adults was restricted to osteolineage cells (Park et al., 2012). Because of the rapid turnover of *Osx*-recombined preosteoblasts, we continuously administered tamoxifen via a chow diet. Although healthy controls exhibited robust labeling of cuboidal bone-lining cells, the number of mature cuboidal osteoblasts in leukemic mice were markedly decreased (Figures 3F and S2B). In addition, we observed in the endosteal region of leukemic mice a striking accumulation of reticular *Osx*-marked cells with cellular extensions toward endothelial cells (Figure 3F) similar to previously described osteoblast precursors in developing bone and in fracture healing (Maes et al., 2010). These reticular *Osx*-labeled cells from leukemic marrow expressed LepR, unlike mature osteoblast from healthy mice (Figures 3G, 3H, and S2C), but lacked osteocalcin expression (Figures 3I and S2D). The decrease in mature osteoblasts in leukemic mice was reflected by significant reduction of mineralized trabecular bone volumes as determined by micro-CT analyses (Figures 3J–3L). Altogether, these results suggest that AML leads to increased bone remodeling with accumulation of osteoblast-primed MSPCs accompanied by reduced numbers of mature bone-forming osteoblasts.

AML Impairs HSC Niche Function

AML often leads to pancytopenia and reductions of normal hematopoiesis, but the mechanisms remain unclear. Next, we evaluated the impact of AML infiltration on HSC niche function of the bone marrow. Sorted stromal PDGFRα^+CD51$^+$ leukemic MSPCs expressed lower levels of *Vcam1*, *Cxcl12*, *Angpt1*, and *Scf* transcripts in comparison to those of healthy controls (Figure 4A). In

Figure 2. Bone Marrow MSPCs and Endothelial Cells Significantly Expand in AML

(A) Left, representative flow cytometry plots, gated on stromal (CD45$^-$Ter119$^-$CD11b$^-$CD31$^-$) bone marrow cells, showing *Nes*-GFP$^+$ cells in control and leukemic mice. Middle and right, frequency and absolute numbers of *Nes*-GFP$^+$ cells per femur (n = 9–10).

(B) Summary of mesenchymal surface marker screening expressed by stromal *Nes*-GFP$^+$ bone marrow cells from leukemic mice (red columns) and healthy controls (gray columns) as detected by flow cytometry analysis (n = 3–10).

(C) Representative flow cytometry plots and quantification of PDGFRα and CD51 double-positive bone marrow stromal cells (n = 9–15).

(D) Cell-cycle analysis of PDGFRα and CD51 double-positive bone marrow stromal cells; representative plots and quantification by flow cytometry with anti-Ki67 and Hoechst 33342 staining (n = 3).

(E) Top, z stack confocal images of thick bone sections stained with anti-Perilipin and Hoechst 33342. The scale bar represents 300 μm. Bottom, frequency of PDGFRα and CD51 double-positive bone marrow stromal cells (left, normalized to control) and quantification of Perilipin$^+$ adipocytes in 0.5 mm^2 area under the growth plate (right) 6 days after sublethal irradiation (n = 4).

(F) Left, frequency of nonhematopoietic (CD45$^-$Ter119$^-$) CD31$^+$ endothelial cells (n = 6). Right, z stack confocal images of thick bone sections stained in vivo with anti-PECAM1 and VE-cadherin antibodies. The magnified confocal images within the area were defined by the rectangle. The scale bar represents 500 μm.

(G) Cell-cycle analysis of endothelial cells quantified by flow cytometry with anti-Ki67 and Hoechst 33342 staining (n = 3). *p < 0.05, **p < 0.01, ***p < 0.001 determined by Student's t test. Data are shown as mean ± SEM.

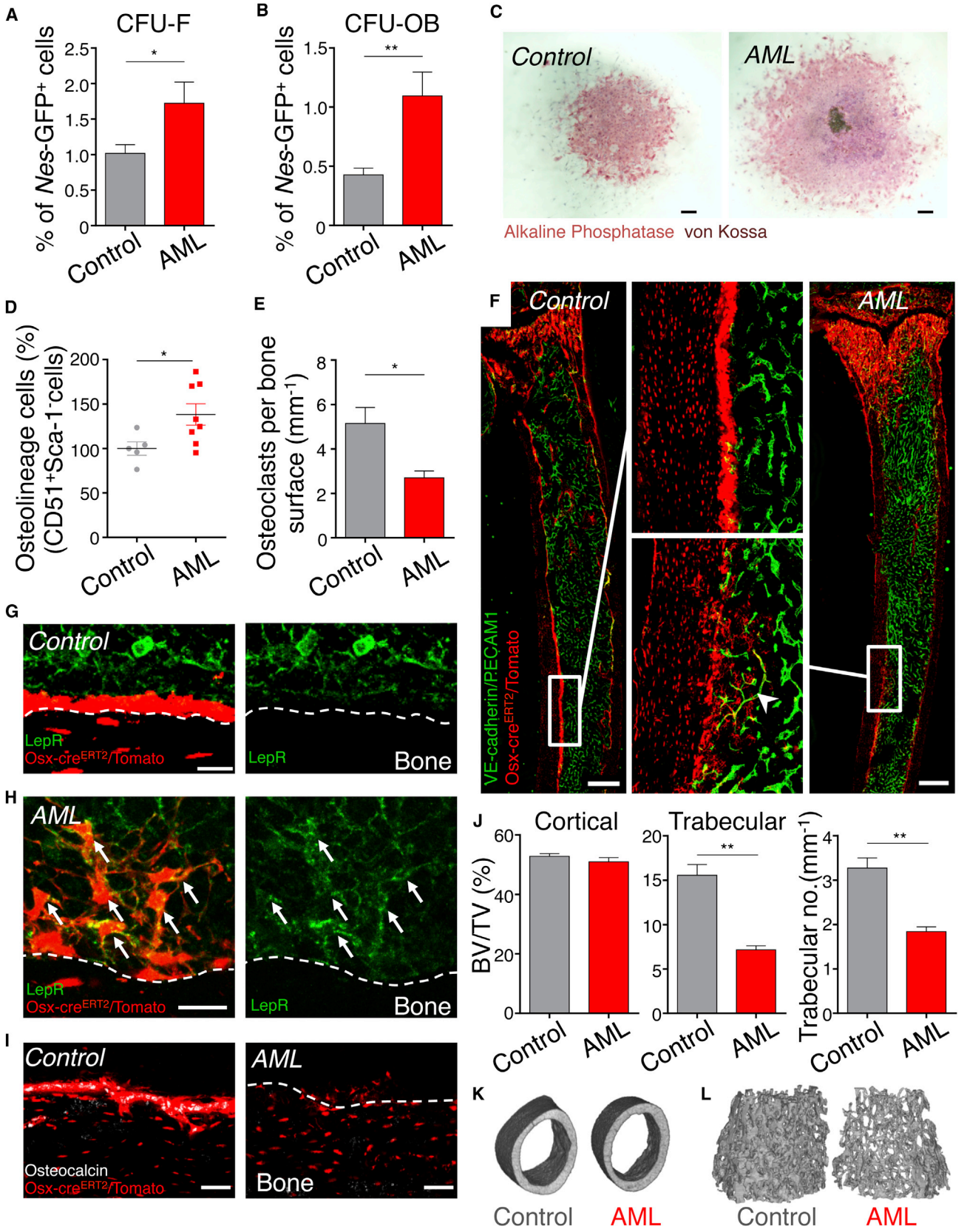

(legend on next page)

contrast, *Opn* expression was increased in bone marrow MSPCs, which is in accordance with their propensity to differentiate into the osteoblastic lineage. In addition, the number of rare pericytic NG2$^+$ cells associated with HSC quiescence and maintenance (Kunisaki et al., 2013) were significantly reduced in leukemic mice (Figures 4B and S3A–S3C). Notably, the reduction of NG2$^+$ cells was not likely due to increased differentiation to the more abundant PDGFRα and CD51 double-positive MSPC population, given that they were not fate mapped by *NG2-cre^{ERTM}/loxp-tdTomato* mice (Figures S3A and S3D). Consistent with reduced numbers of periarteriolar NG2$^+$ cells and lower levels of HSC-regulating genes, phenotypic long-term HSCs initially expanded, but were then significantly reduced, in the bone marrow of leukemic mice (Figures 4C and S3E). The reduction of functional HSCs and hematopoietic progenitor cells in the bone marrow was confirmed by long-term culture-initiating cell (LTC-IC) assays (Figures 4D and 4E), CFU-Cs and phenotypic progenitors (Figures 4G and S3G), and competitive repopulation assays (Figure S3F). The reduced expression of HSC maintenance and retention genes (Figure 4A) in *Nes*$^+$ cells led to significant mobilization of phenotypic HSCs and colony-forming progenitors to the circulation and the spleen (Figures 4F, S3H, and S3I). In addition, whole-mount imaging analyses revealed that bone marrow HSCs were displaced away from arterioles (Figure 4H). Thus, these results strongly suggest that AML severely alters the niche, leading to reduced ability to maintain healthy HSC in the bone marrow.

Stromal β2 Adrenergic Receptors Regulate LSCs

Previous studies have shown that the SNS regulates bone formation through β2 adrenergic receptors expressed on osteoblasts (Elefteriou et al., 2005; Takeda et al., 2002), whereas β3 adrenergic signaling appears to play a more prominent role in regulating the healthy HSC niche (Méndez-Ferrer et al., 2008). Consistent with the enhanced osteolineage differentiation of MSPCs in AML, the expression of the *Adrβ3* in PDGFRα^+CD51$^+$ stromal cells was significantly reduced in comparison to healthy mice, whereas the *Adrβ2* expression remained unchanged (Figure S4A). To get additional mechanistic insight into SNS regulation of leukemia formation, we treated mice with specific Adrβ2 (ICI118,551) and Adrβ3 (SR59230A) antagonists starting 3 days prior to transplantation. We found that the inhibition of Adrβ2, but not Adrβ3, significantly augmented the numbers of phenotypic LSCs in the bone marrow in comparison to control mice (Figure 4I). Leukemic bone marrow cells from ICI118,551-treated mice exhibited significantly higher colony-forming capacity and also formed significantly larger colonies, indicating greater proliferative capacity (Figure S4B). Increased leukemic infiltration by the blockade of Adrβ2 was associated with significantly reduced survival of leukemic mice (Figure 4J). Given that Adrβ2 is also expressed on leukemic cells (data not shown), we sought to ascertain whether sympathetic signals directly regulated AML cells or whether the signals were mediated through the microenvironment. To this end, we transplanted MLL-AF9 leukemic cells (expressing the Adrβ2) into Adrβ2-deficient or -sufficient animals. We observed a significantly higher leukemic bone marrow infiltration in Adrβ2-deficient mice, suggesting a critical role for Adrβ2 expressed in the microenvironment (Figure 4K). Conversely, the administration of an Adrβ2 agonist (Clenbuterol hydrochloride) led to a significant reduction of phenotypic LSCs in bone marrow, spleen, and blood and tended to prolong survival (Figures 4L and S4C–S4E). However, Clenbuterol also had a different cell-autonomous action, given that it enhanced in vitro proliferation of MLL-AF9 cells (Figure S4F). Thus, these results suggest that, although β2 agonist might rescue the healthy niche to limit LSC expansion, it also has an opposite action on leukemia cells that may mitigate its antileukemic effects.

DISCUSSION

Here, we show that MLL-AF9 AML rapidly transforms the HSC niche, reducing the numbers of arteriole-associated NG2$^+$ niche cells and the density of their SNS nerve network, which is critical for MSC quiescence. This leads to the expansion of *Nes*-GFP$^+$ niche cells committed to differentiate toward the osteoblast lineage with a block of differentiation to mature osteoblasts. The high expression of *Opn* by leukemic niche cells is also consistent with osteoblastic commitment and may contribute to AML progression, as recently reported in an ALL model (Boyerinas et al., 2013), and because the major Opn receptor, $\alpha_V\beta_3$ integrin,

Figure 3. Bone Marrow *Nes*-GFP$^+$ MSPCs Have Differentiated Toward the Osteoblastic Lineage

(A and B) Stromal *Nes*-GFP$^+$ cells were sorted from control and leukemic bone marrow and plated at equal numbers at clonal densities under CFU-F and CFU-OB culture conditions. Frequency of CFU-F (n = 6–7, in duplicate and triplicate per mouse; A) and CFU-OB (n = 4–5, in triplicate per mouse; B) from bone marrow *Nes*-GFP$^+$ cells.

(C) Representative images of CFU-OB colonies from *Nes*-GFP$^+$ bone marrow cells stained with alkaline phosphatase and von Kossa and counterstained with hematoxylin. The scale bar represents 500 μm.

(D) Absolute numbers of stromal CD51$^+$/Sca-1$^-$ osteolineage cells in the compact bone (normalized to control, n = 5–8).

(E) Quantification of TRAP$^+$ osteoclasts in the metaphyseal area (500 μm under the growth plate area) of the tibia. Number of TRAP$^+$ cells in relation to the measured bone surface (n = 3).

(F) Z stack confocal images of thick bone sections of *Osterix-cre^{ERT2}/loxp-tdTomato* control and leukemic mice. Middle, the magnified confocal images within the area defined by the rectangle. Arrowhead indicates osteoblast precursors. Anti-PECAM1 and VE-cadherin antibodies in vivo. The scale bar represents 500 μm.

(G and H) Z stack confocal images of thick bone sections of *Osterix-cre^{ERT2}/loxp-tdTomato* control (G) and leukemic (H) mice stained with anti-LepR (arrows denote LepR-expressing Osx-Cre/Tomato$^+$ cells). The scale bar represents 20 μm.

(I) Z stack confocal images of thick bone sections of *Osterix-cre^{ERT2}/loxp-tdTomato* control (left) and leukemic (right) mice stained with osteocalcin antibody. The scale bar represents 50 μm.

(J) Micro-CT analysis of femurs from control and leukemic mice (n = 3). Analysis of cortical (left) and trabecular (middle) bone volume/total volume (BV/TV) as well as trabecular number (right).

(K and L) Representative micro-CT images of cortical (K) and trabecular (L) bone from control and leukemic mice. *$p < 0.05$, **$p < 0.01$ determined by the Student's t test. Data are shown as mean ± SEM.

See also Figure S2.

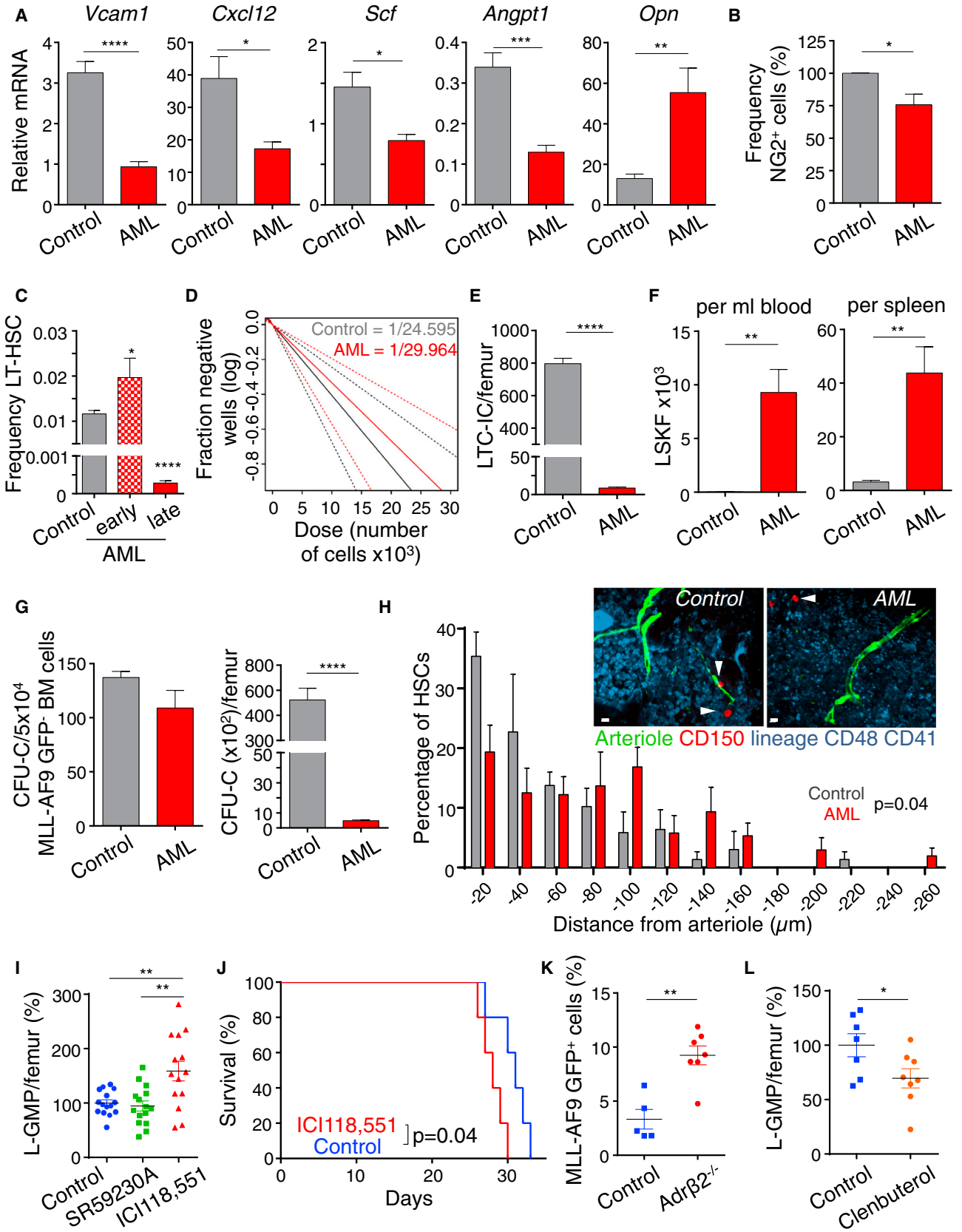

(legend on next page)

is expressed by MLL-AF9 AML cells and was shown to be required for leukemogenesis (Miller et al., 2013). Our results suggest that sympathetic neuropathy represents a mechanism by which AML co-opts the microenvironment to its own advantage to deplete niche cells that maintain healthy HSCs and expand leukemia-supportive, more differentiated, $Nes^{+}LepR^{+}$ *Osx*-cre^{ERT2}-labeled mesenchymal progenitors. Finally, the decreased sympathetic tone in bone marrow and spleen reinforces leukemia progression through an altered niche.

A recent study has suggested that the microenvironment of leukemias can be differentially regulated wherein increased osteoblastic function (by activation of the parathyroid hormone receptor) is associated with progression of MLL-AF9 AML, whereas *BCR-ABL*-driven disease was markedly attenuated (Krause et al., 2013). It is notable that BCR-ABL CML blast crisis—which resembles acute leukemia—led to significant reductions of mature osteoblasts (Frisch et al., 2012), whereas in a more chronic model of BCR-ABL CML, bone-forming mature osteoblasts were reportedly increased (Schepers et al., 2013), suggesting that AML and CML may have opposing effects on differentiation to mature osteoblasts.

Our results shed light on the mechanisms by which MLL-AF9 AML cells remodel the bone marrow niche in order to create a self-sustaining microenvironment at the expense of the maintenance of healthy HSCs. Thus, manipulation of the adrenergic system or other pathways that prevent mesenchymal differentiation may provide a potentially powerful strategy for limiting LSC development and preserving healthy HSCs.

EXPERIMENTAL PROCEDURES

Detailed procedures can be found in the Supplemental Experimental Procedures.

Mouse Strains

All murine experiments were performed with adult 6- to 10-week-old animals. All mice were housed in specific pathogen-free facilities at the Albert Einstein College of Medicine animal facility, and all experimental procedures were approved by the Animal Care and Use Committee of the Albert Einstein College of Medicine. C57BL/6 mice were purchased from National Cancer Institute (Frederick Cancer Research Center). Cspg4-DsRed.T1 (*NG2*DsRed), B6.Cg-*Gt(ROSA)26Sor*$^{tm14(CAG-tdTomato)Hze}$/J (*loxp-tdTomato*), and B6.Cg-Tg(Cspg4-cre/Esr1*)BAkik/J (*NG2-*cre^{ERTM}) mice were purchased from the Jackson Laboratory. *Nes-Gfp* transgenic mice (Mignone et al., 2004) and *NOD-scid Il2Rg*$^{-/-}$ (NSG) mice were bred and used at the Albert Einstein College of Medicine. *Osx-*cre^{ERT2} mice (Maes et al., 2010) were kindly provided by Dr. Henry M. Kronenberg and backcrossed for five generations into C57BL/6 background. *Adrb2*^{tm1Bkk} were a gift from Dr. Gerard Karsenty.

In Vivo Treatments

For induction of Cre-mediated recombination in *Osx-*Cre^{ERT2} mice, chow diet (Harlan Laboratories) containing tamoxifen (Sigma-Aldrich) at 750 mg/kg with 5% sucrose was given. For induction of Cre-mediated recombination in *NG2-*Cre^{ERTM} mice, 1 mg tamoxifen (Sigma-Aldrich) was injected twice daily for 5 consecutive days as previously described (Kunisaki et al., 2013). For denervation experiments, 6OHDA was intraperitoneally (i.p.) given at 24 hr (100 mg/kg) and 72 hr (250 mg/kg) after transplantation unless otherwise stated. The β2-specific antagonist ICI 118,551 hydrochloride (1 mg/kg body weight i.p.) and the β3-specific antagonist SR59230A (5 mg/kg body weight i.p.) were given daily beginning 3 days prior to transplantation, and Clenbuterol hydrochloride (2 mg/kg body weight s.c.) was given daily 3 days after transplantation (all from Sigma-Aldrich).

Statistical Analyses

All data are shown as the mean ± SEM. Unless otherwise indicated for comparisons between two groups, the Student's t test was applied. Log-rank analyses were used for Kaplan-Meier survival curves. Analyses were performed with GraphPad Prism software. *$p < 0.05$, **$p < 0.01$, ***$p < 0.001$, ****$p < 0.0001$.

SUPPLEMENTAL INFORMATION

Supplemental Information contains Supplemental Experimental Procedures and four figures and can be found with this article online at http://dx.doi.org/10.1016/j.stem.2014.06.020.

ACKNOWLEDGMENTS

We thank Colette Prophete, Lauren Schiff, Paul Ciero, Matthew Huggins, Sana Mohamad, and Michael Möllmann for technical assistance; the Stem Cell FACS Facility and Einstein Flow Cytometry Core Facility for expert cell sorting; Dr. Luis Cardoso for micro-CT analyses; Dr. Raymond Johnson for noradrenaline measurements; Dr. Rani Sellers for histopathological examinations; and

Figure 4. Leukemic Bone Marrow Niche Has Impaired HSC-Regulating Capacity and Regulates LSCs through the β2 Adrenergic Receptor

(A) Gene expression analysis of key HSC-regulatory genes (*Vcam1*, *Cxcl12*, *Angpt1*, *Scf*, and *Opn*) in sorted bone marrow $PDGFR\alpha^{+}/CD51^{+}$ stromal cells by real-time PCR (n = 5–6).

(B) Frequency of stromal $NG2DsRed^{+}$ cells in the bone marrow (normalized to control, n = 6–7).

(C) Frequency of phenotypic $Lin^{-}Sca\text{-}1^{+}c\text{-}kit^{+}Flt3^{-}CD34^{-}$ long-term HSCs in leukemic mice with 86.5% mean bone marrow infiltration (early) and >95% bone marrow infiltration (late) in comparison to matched control mice (n = 10, 5, and 8).

(D) Quantification of long-term reconstituting HSCs by LTC-IC assay on sorted GFP^{-} cells isolated from control and late stage leukemic mice. Estimated LTC-IC frequency is given. Dashed lines represent 95% confidence interval.

(E) LTC-IC numbers per femur calculated with the frequency of MLL-AF9 GFP^{-} cells in the bone marrow (n = 3–5).

(F) Absolute numbers of $Lin^{-}Sca\text{-}1^{+}c\text{-}kit^{+}Flt3^{-}$ (LSKF) cells in peripheral blood (left) and spleen (right; n = 4–5) in leukemic (mean bone marrow infiltration = 86.5%) and matched control mice.

(G) Left, CFU-C from 5×10^{4} sorted MLL-AF9 GFP^{-} bone marrow (BM) cells. Right, CFU-C numbers per femur calculated with the frequency of MLL-AF9 GFP^{-} cells (n = 5–6).

(H) Representative whole-mount images and distribution of HSCs in the sternal bone marrow relative to *Nes*-GFP^{bright} arterioles (n = 54; 75 HSCs per control and AML [late stage] group, respectively). Arrowheads denote HSCs. Two-sample Kolmogorov-Smirnov test, p = 0.04. The scale bar represents 10 μm.

(I) Absolute number of L-GMPs per femur in mice treated with the Adrβ3-inhibitor (SR59230A), Adrβ2 inhibitor (ICI118,551), and control leukemic mice 18 days after transplantation (normalized to control, n = 14–15).

(J) Survival curve of mice treated with ICI118,551 and control mice (n = 5).

(K) Frequency of leukemic cells per femur in *Adrβ2*$^{-/-}$ and control mice (n = 5–7).

(L) Absolute number of L-GMPs per femur in mice treated with the Adrβ2 agonist (Clenbuterol hydrochloride) and control leukemic mice 19 days after transplantation (normalized to control, n = 7–8). *$p < 0.05$, **$p < 0.01$, ***$p < 0.001$, ****$p < 0.0001$ determined by the Student's t test. Data are shown as mean ± SEM. See also Figures S3 and S4.

Dr. Britta Will for helpful scientific discussions. This work was supported by R01 grants from the National Institutes of Health (DK056638, HL116340, and HL097819 to P.S.F), the New York Stem Cell Foundation, and the National Cancer Institute (CA140575 and CA66996 to S.A.A.). M.H. is supported by a fellowship of the German Research Foundation (DFG, Ha 6731/1-1), S.P. is a New York Stem Cell Foundation-Druckenmiller Fellow, and H.P. is supported by a Training Program in Cellular and Molecular Biology and Genetics (T32 GM007491).

Received: December 23, 2013
Revised: May 21, 2014
Accepted: June 30, 2014
Published: July 10, 2014

REFERENCES

Aguayo, A., Kantarjian, H., Manshouri, T., Gidel, C., Estey, E., Thomas, D., Koller, C., Estrov, Z., O'Brien, S., Keating, M., et al. (2000). Angiogenesis in acute and chronic leukemias and myelodysplastic syndromes. Blood *96*, 2240–2245.

Boyerinas, B., Zafrir, M., Yesilkanal, A.E., Price, T.T., Hyjek, E.M., and Sipkins, D.A. (2013). Adhesion to osteopontin in the bone marrow niche regulates lymphoblastic leukemia cell dormancy. Blood *121*, 4821–4831.

Bryon, P.A., Gentilhomme, O., and Fiere, D. (1979). [Histomorphometric analysis of bone-marrow adipose density and heterogeneity in myeloid aplasia and dysplasia (author's transl)]. Pathol. Biol. (Paris) *27*, 209–213.

Byrd, J.C., Mrózek, K., Dodge, R.K., Carroll, A.J., Edwards, C.G., Arthur, D.C., Pettenati, M.J., Patil, S.R., Rao, K.W., Watson, M.S., et al.; Cancer and Leukemia Group B (CALGB 8461) (2002). Pretreatment cytogenetic abnormalities are predictive of induction success, cumulative incidence of relapse, and overall survival in adult patients with de novo acute myeloid leukemia: results from Cancer and Leukemia Group B (CALGB 8461). Blood *100*, 4325–4336.

Colmone, A., Amorim, M., Pontier, A.L., Wang, S., Jablonski, E., and Sipkins, D.A. (2008). Leukemic cells create bone marrow niches that disrupt the behavior of normal hematopoietic progenitor cells. Science *322*, 1861–1865.

Ding, L., Saunders, T.L., Enikolopov, G., and Morrison, S.J. (2012). Endothelial and perivascular cells maintain haematopoietic stem cells. Nature *481*, 457–462.

Elefteriou, F., Ahn, J.D., Takeda, S., Starbuck, M., Yang, X., Liu, X., Kondo, H., Richards, W.G., Bannon, T.W., Noda, M., et al. (2005). Leptin regulation of bone resorption by the sympathetic nervous system and CART. Nature *434*, 514–520.

Ferrara, F., and Schiffer, C.A. (2013). Acute myeloid leukaemia in adults. Lancet *381*, 484–495.

Frenette, P.S., Pinho, S., Lucas, D., and Scheiermann, C. (2013). Mesenchymal stem cell: keystone of the hematopoietic stem cell niche and a stepping-stone for regenerative medicine. Annu. Rev. Immunol. *31*, 285–316.

Frisch, B.J., Ashton, J.M., Xing, L., Becker, M.W., Jordan, C.T., and Calvi, L.M. (2012). Functional inhibition of osteoblastic cells in an in vivo mouse model of myeloid leukemia. Blood *119*, 540–550.

Gronthos, S., Zannettino, A.C., Hay, S.J., Shi, S., Graves, S.E., Kortesidis, A., and Simmons, P.J. (2003). Molecular and cellular characterisation of highly purified stromal stem cells derived from human bone marrow. J. Cell Sci. *116*, 1827–1835.

Hussong, J.W., Rodgers, G.M., and Shami, P.J. (2000). Evidence of increased angiogenesis in patients with acute myeloid leukemia. Blood *95*, 309–313.

Ishikawa, F., Yoshida, S., Saito, Y., Hijikata, A., Kitamura, H., Tanaka, S., Nakamura, R., Tanaka, T., Tomiyama, H., Saito, N., et al. (2007). Chemotherapy-resistant human AML stem cells home to and engraft within the bone-marrow endosteal region. Nat. Biotechnol. *25*, 1315–1321.

Katayama, Y., Battista, M., Kao, W.M., Hidalgo, A., Peired, A.J., Thomas, S.A., and Frenette, P.S. (2006). Signals from the sympathetic nervous system regulate hematopoietic stem cell egress from bone marrow. Cell *124*, 407–421.

Krause, D.S., Fulzele, K., Catic, A., Sun, C.C., Dombkowski, D., Hurley, M.P., Lezeau, S., Attar, E., Wu, J.Y., Lin, H.Y., et al. (2013). Differential regulation of myeloid leukemias by the bone marrow microenvironment. Nat. Med. *19*, 1513–1517.

Krivtsov, A.V., Twomey, D., Feng, Z., Stubbs, M.C., Wang, Y., Faber, J., Levine, J.E., Wang, J., Hahn, W.C., Gilliland, D.G., et al. (2006). Transformation from committed progenitor to leukaemia stem cell initiated by MLL-AF9. Nature *442*, 818–822.

Kunisaki, Y., Bruns, I., Scheiermann, C., Ahmed, J., Pinho, S., Zhang, D., Mizoguchi, T., Wei, Q., Lucas, D., Ito, K., et al. (2013). Arteriolar niches maintain haematopoietic stem cell quiescence. Nature *502*, 637–643.

Lane, S.W., Wang, Y.J., Lo Celso, C., Ragu, C., Bullinger, L., Sykes, S.M., Ferraro, F., Shterental, S., Lin, C.P., Gilliland, D.G., et al. (2011). Differential niche and Wnt requirements during acute myeloid leukemia progression. Blood *118*, 2849–2856.

Lucas, D., Scheiermann, C., Chow, A., Kunisaki, Y., Bruns, I., Barrick, C., Tessarollo, L., and Frenette, P.S. (2013). Chemotherapy-induced bone marrow nerve injury impairs hematopoietic regeneration. Nat. Med. *19*, 695–703.

Maes, C., Kobayashi, T., Selig, M.K., Torrekens, S., Roth, S.I., Mackem, S., Carmeliet, G., and Kronenberg, H.M. (2010). Osteoblast precursors, but not mature osteoblasts, move into developing and fractured bones along with invading blood vessels. Dev. Cell *19*, 329–344.

Magnon, C., Hall, S.J., Lin, J., Xue, X., Gerber, L., Freedland, S.J., and Frenette, P.S. (2013). Autonomic nerve development contributes to prostate cancer progression. Science *341*, 1236361.

Medyouf, H., Mossner, M., Jann, J.C., Nolte, F., Raffel, S., Herrmann, C., Lier, A., Eisen, C., Nowak, V., Zens, B., et al. (2014). Myelodysplastic cells in patients reprogram mesenchymal stromal cells to establish a transplantable stem cell niche disease unit. Cell Stem Cell *14*, 824–837.

Méndez-Ferrer, S., Lucas, D., Battista, M., and Frenette, P.S. (2008). Haematopoietic stem cell release is regulated by circadian oscillations. Nature *452*, 442–447.

Méndez-Ferrer, S., Michurina, T.V., Ferraro, F., Mazloom, A.R., Macarthur, B.D., Lira, S.A., Scadden, D.T., Ma'ayan, A., Enikolopov, G.N., and Frenette, P.S. (2010). Mesenchymal and haematopoietic stem cells form a unique bone marrow niche. Nature *466*, 829–834.

Mignone, J.L., Kukekov, V., Chiang, A.S., Steindler, D., and Enikolopov, G. (2004). Neural stem and progenitor cells in nestin-GFP transgenic mice. J. Comp. Neurol. *469*, 311–324.

Miller, P.G., Al-Shahrour, F., Hartwell, K.A., Chu, L.P., Järås, M., Puram, R.V., Puissant, A., Callahan, K.P., Ashton, J., McConkey, M.E., et al. (2013). In Vivo RNAi screening identifies a leukemia-specific dependence on integrin beta 3 signaling. Cancer Cell *24*, 45–58.

Mizoguchi, T., Pinho, S., Ahmed, J., Kunisaki, Y., Hanoun, M., Mendelson, A., Ono, N., Kronenberg, H.M., and Frenette, P.S. (2014). Osterix marks distinct waves of primitive and definitive stromal progenitors during bone marrow development. Dev. Cell *29*, 340–349.

Padró, T., Ruiz, S., Bieker, R., Bürger, H., Steins, M., Kienast, J., Büchner, T., Berdel, W.E., and Mesters, R.M. (2000). Increased angiogenesis in the bone marrow of patients with acute myeloid leukemia. Blood *95*, 2637–2644.

Park, D., Spencer, J.A., Koh, B.I., Kobayashi, T., Fujisaki, J., Clemens, T.L., Lin, C.P., Kronenberg, H.M., and Scadden, D.T. (2012). Endogenous bone marrow MSCs are dynamic, fate-restricted participants in bone maintenance and regeneration. Cell Stem Cell *10*, 259–272.

Pinho, S., Lacombe, J., Hanoun, M., Mizoguchi, T., Bruns, I., Kunisaki, Y., and Frenette, P.S. (2013). PDGFRα and CD51 mark human nestin+ sphere-forming mesenchymal stem cells capable of hematopoietic progenitor cell expansion. J. Exp. Med. *210*, 1351–1367.

Schepers, K., Pietras, E.M., Reynaud, D., Flach, J., Binnewies, M., Garg, T., Wagers, A.J., Hsiao, E.C., and Passegué, E. (2013). Myeloproliferative

neoplasia remodels the endosteal bone marrow niche into a self-reinforcing leukemic niche. Cell Stem Cell *13*, 285–299.

Sugiyama, T., Kohara, H., Noda, M., and Nagasawa, T. (2006). Maintenance of the hematopoietic stem cell pool by CXCL12-CXCR4 chemokine signaling in bone marrow stromal cell niches. Immunity *25*, 977–988.

Takeda, S., Elefteriou, F., Levasseur, R., Liu, X., Zhao, L., Parker, K.L., Armstrong, D., Ducy, P., and Karsenty, G. (2002). Leptin regulates bone formation via the sympathetic nervous system. Cell *111*, 305–317.

Wei, J., Wunderlich, M., Fox, C., Alvarez, S., Cigudosa, J.C., Wilhelm, J.S., Zheng, Y., Cancelas, J.A., Gu, Y., Jansen, M., et al. (2008). Microenvironment determines lineage fate in a human model of MLL-AF9 leukemia. Cancer Cell *13*, 483–495.

Winkler, I.G., Sims, N.A., Pettit, A.R., Barbier, V., Nowlan, B., Helwani, F., Poulton, I.J., van Rooijen, N., Alexander, K.A., Raggatt, L.J., and Lévesque, J.P. (2010). Bone marrow macrophages maintain hematopoietic stem cell (HSC) niches and their depletion mobilizes HSCs. Blood *116*, 4815–4828.

Zhang, B., Ho, Y.W., Huang, Q., Maeda, T., Lin, A., Lee, S.U., Hair, A., Holyoake, T.L., Huettner, C., and Bhatia, R. (2012). Altered microenvironmental regulation of leukemic and normal stem cells in chronic myelogenous leukemia. Cancer Cell *21*, 577–592.